Theory of single atom manipulation with a scanning probe tip: Force signatures, constant-height, and constant-force scans

Laurent Pizzagalli*

Laboratoire de Métallurgie Physique, UMR 6630, Université de Poitiers, SP2MI, Boîte Postal 30179, 86962 Futuroscope Chasseneuil Cedex, France

Alexis Baratoff

Department of Physics and Astronomy, Basel University, Klingelbergstrasse 82, CH-4056 Basel, Switzerland

We report theoretical results predicting the atomic manipulation of a silver atom on a Si(001) surface by a scanning probe tip, and providing insight into the manipulation phenomena. A molecular mechanics technique has been used, the system being described by a quantum chemistry method for the short-range interactions and an analytical model for the long-range ones. Taking into account several shapes, orientations, and chemical natures of the scanning tip, we observed four different ways to manipulate the deposited atom in a constant-height mode. In particular, the manipulation is predicted to be possible with a Si(111) tip for different tip shapes and adatom locations on the silicon surface. The calculation of the forces during the manipulation revealed that specific variations can be associated with each kind of process. These force signatures, such as the tip height signatures observed in scanning tunneling microscope experiments, could be used to deduce the process involved in an experiment. Finally, we present preliminary results about the manipulation in constant-force mode.

PACS number(s): 81.16.Ta, 82.37.Gk, 02.70.Ns, 68.43.Fg

I. INTRODUCTION

Originally designed to image surfaces, scanning probe techniques[1–3] have also rapidly proved to be efficient for acting on the surfaces at the nanoscopic scale.[4] First evidences came from the observation of the consequences of the contact between the scanning probe tip and the studied surface. For instance, Li *et al.* observed that the mechanical interaction between their scanning tunneling microscope (STM) tungsten tip and one Au surface led to the creation of nanoscopic pits.[5] Similar indentation has also been performed on dichalcogenide WSe_2 surfaces.[6,7] Another kind of nanopatterning was achieved by the formation of mounds on the surface by field-emitting gold tip atoms.[8] Dimensions of these created nanostructures were typically 100–300 Å. However, manipulation with scanning probe techniques made a major step when state-of-the-art experiments performed in the group of Eigler have shown that the STM tip could even control a unique deposited atom with an impressive accuracy.[9] According to the notation of Stroscio and Eigler, manipulation processes can be classified into two categories.[10] *Vertical* processes involve atom transfers between the tip and the surface, voltage pulse or direct tip-surface contact being used for the atom transfers. Adsorbates or native surface atoms can be either permanently extracted by the tip[11–22] or redeposited in another location.[23–26] This mode has been theoretically studied by several groups.[27–33] In the *lateral* category, manipulated objects always stay on the surface.[10] It is the scanning probe tip which either (i) traps the object in the surroundings of its apex and slides it,[9,25,34,35] (ii) pushes the object along the scan path,[36–42] or (iii) controls the diffusion by voltage pulse.[43,44]

It seems that the potential of lateral manipulation has not been completely explored. Successful experiments have been performed for very small objects, such as Xe atoms on Ni(110),[9] CO molecules and Pt atoms on Pt(111),[34] Cu, Pb atoms, and CO, Pb_2, C_2H_4 molecules on Cu(211).[25,35,45] However, in these studies, all supporting substrates are closed metallic surfaces. Their low diffusion energy barriers make the manipulation easier. Theoretically, several calculations of the lateral manipulation of one atom have been done, and it has been found that single atoms can be manipulated on metallic [Pt(111),[32] Cu(110),[46,47] Cu(211)[48]] or insulating [NaCl(001) Ref. 49] substrates. However, only one kind of tip is usually considered, which limits the scope of the results. Another limitation concerns the substrate. To our knowledge, the manipulation of one unique atom on a surface having a significant technological importance has not been achieved yet. The Si(001) surface, heavily used in the electronic industry, is an interesting and still unprobed candidate. In a previous paper, preliminary calculations had shown that one single Ag atom deposited on the Si(001) surface may be manipulated by a tip during a constant-height scan.[50] The complete results of the study are presented and discussed in this paper. First, we focus on constant-height manipulation. In particular, we analyze the influence of several parameters, such as the shape of the tip, its orientation, and its chemical composition. Second, we show original results about the variation of the forces acting on the tip during different manipulation processes. These variations are then discussed in relation with the recent works on STM current signatures.[35,51,52] Finally, in the last section, we discuss the possibility to perform constant-force manipulation scans with an atomic force microscope (AFM) tip, and we show some examples.

II. MODELS

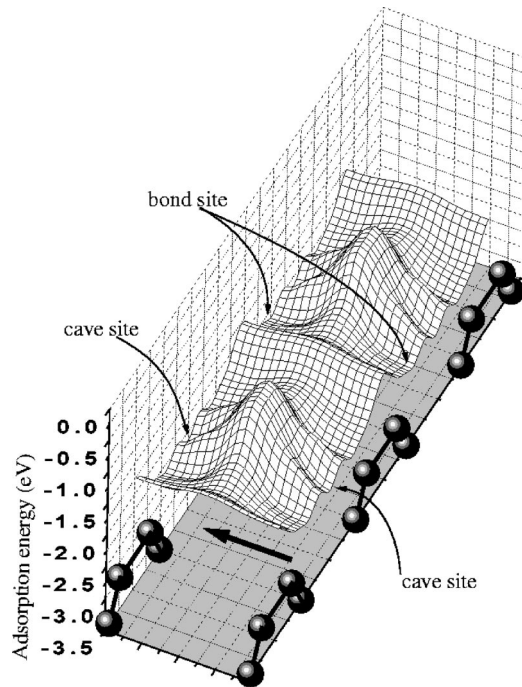The silicon (001) surface is now very well understood, thanks to several experimental[53–55] and theoretical

FIG. 1. Adsorption energy map of one Ag deposited on Si(001)-2×1. The black spheres represent the Si surface and subsurface atoms. The bold arrow shows the tip movement direction.

studies.[56–58] In its ground state, the surface is $c(4\times2)$ reconstructed, with alternating asymmetric dimers. A (2×1) reconstruction is observed at room temperature because the asymmetric dimers oscillate very rapidly and appear to be symmetric on the time scale of experiments. When a silver atom is deposited on the Si(001) surface, most of the experimental studies agreed that the adatom adsorbs preferentially in the cave site, i.e., between two Si dimers belonging to two adjacent dimer rows.[59–63] In Fig. 1, we have represented the adsorption energy map for one Ag atom deposited on the Si(001) surface.[64] The cave site is the most stable, though its corresponding adsorption energy is very close to the energy of the bond site (Ag atom bonded to one dimerized Si atoms). This quasidegeneracy could explain why the Ag atom is sometimes found in the bond site.[65] Here, most of the calculations have been carried out with the silver atom initially adsorbed in the cave site. However, we have also considered the case of adsorption in the bond site for selected examples.

Two complementary models have been used to represent our system, which is composed of the scanning probe tip, the Ag atom, and the Si(001) surface. First, the short-range
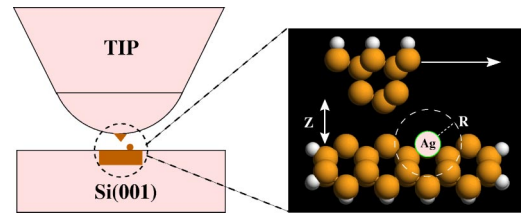

FIG. 2. Models used in the calculations. The left panel represents the geometrical shapes (light gray) from which long-range van der Waals forces are estimated. The small dark gray region shows the very end of the scanning tip, the adatom and the surface beneath which are treated by an extended Hückel calculation to account for the chemical bondings. A ball-and-stick model of this region shows the clusters used to represent the surface and the Si(111) tip (right panel).

chemical forces between the very end of the tip, the adatom and the surface are described by the atom superposition and electron delocalization (ASED) method.[66] This extension of the extended Hückel molecular orbitals (EHMO) model has been successfully used for the study of adsorption on silicon surfaces.[67] In addition, it allows to describe the interactions between several different species within a uniform and coherent scheme. *Ab initio* methods have the same advantage, but the systematic study of several manipulation conditions with a realistic system is still an unfeasible task. In our calculations, the silicon surface is represented by a four-layer cluster, each layer encompassing 4×4 Si atoms (eight Si dimers). Hydrogen atoms are added to passivate the bottom and the sides of the slab, leaving a clean Si(001) surface on top (see Fig. 2). Careful checks have shown that this cluster size is large enough to avoid unwanted size effects. Relaxation of the bare Si(001) surface with the ASED method leads to a symmetric (2×1) surface instead of the $c(4\times2)$ reconstruction. However, the energy difference between these two structures is very small[58] and within the uncertainty of the ASED model. In addition, the height difference between the "up" and "down" atoms of the asymmetric dimer atoms is also small. Therefore, we expect correct tendencies for manipulation processes involving much larger energies and amplitudes. The tip apex has been modeled using Si and Au clusters built along the (111) orientation, with 13 Si or 10 Au atoms for sharp tips (see Fig. 7). Each Si atom located in the base layer of the pyramidal tip was saturated by a hydrogen atom. All the EHMO parameters used in our calculations are reported in the Table I.

With the second model, we describe the long-range van der Waals forces between the tip and the surface. Although these interactions are the leading forces for the manipulation

TABLE I. EHMO parameters. $\zeta_{s,p,d}$ are the Slater orbital exponents, $IP_{s,p,d}$ the ionization potentials, and $C_{1,2}$ the linear coefficients for double-ζ functions.

	ζ_s	IP_s	ζ_p	IP_p	$\zeta1_d$	IP_d	C_1	$\zeta2_d$	C_2
H	1.1600	−13.600							
Si	1.6998	−13.460	1.4855	−8.151					
Ag	1.9060	−7.580	1.6200	−3.920	4.9890	−10.500	0.5576	2.5840	0.5536
Au	2.6020	−10.920	2.5840	−5.550	6.1630	−15.070	0.6851	2.7940	0.5696

of physisorbed atoms,[46,47,52] these are expected to have a negligible effect in the case of a chemisorbed atom. We can then safely neglect the long-range interactions involving the Ag atom, as well as the very small contributions arising from the tip cluster apex. However, it is essential to take into account the van der Waals interaction between the macroscopic tip and the substrate in order to get a correct force distance relation.[68] It is well known that quantum chemistry methods such as ASED or local-density-aproximation-related techniques are unable to describe the dispersive van der Waals interactions. Here we have used an analytical Hamaker model,[69] with the parametric relation [Eq. (1)] derived from a tip built with an infinite cone[70] and a spherical cap, and an infinite surface. The geometry of the model is shown on the left panel of the Fig. 2. We used a spherical cap radius $\rho = 50$ nm. The Hamaker constant A for the Si-Si interaction is 1.865×10^{-19} J.[71] In Eq. (1), h is actually the distance between the surface and the bottom of the macroscopic tip (without the tip apex cluster), i.e., h is the sum of the distance Z between the surface and the bottom of the tip apex cluster, determined from the center of the atoms, and of the height of the cluster [about 6.4 Å for the Si(111) tip]. With this parametrization, we obtained a maximum attractive van der Waals force of 6.42 nN between the Si tip and the Si surface.

$$F_z(h) = \frac{A\rho^2(1 - \sin\gamma)(\rho\sin\gamma - \rho - h\sin\gamma - h)}{6h^2(\rho + h - \rho\sin\gamma)^2}$$
$$- \frac{A\tan\gamma[h\sin\gamma + \rho\sin\gamma + \rho\cos(2\gamma)]}{6\cos\gamma(\rho + h - \rho\sin\gamma)^2}. \quad (1)$$

In view of the very slow displacement of the tip apex usually achieved experimentally in manipulation as compared to the relaxation time of the adsorbate on a surface, a molecular mechanics approach was preferred to a molecular dynamics approach.[72] For each tip position (X_{tip}, Z_{tip}) considered, the Ag and slab atoms positions are optimized to get the system minimum energy. X_{tip} is the tip apex coordinate along the Si dimer row axis, a zero value referring to the initial location of the silver adatom. In order to avoid time-consuming calculations, only the Ag atom and all the surface silicon atoms closer to Ag than a fixed distance R (see Fig. 2) were allowed to relax. We have checked the validity of this approximation by considering several R distances, from 5 Å to 0 Å (frozen surface). In most of the cases, we used a frozen surface because we got no qualitative changes and nonsignificant quantitative variations. The tip atoms are not allowed to relax, what could be questionable for small tip surface distances. Consequently, our tip was always located high enough to ensure no significant interaction with the surface atoms. In this work, we have considered constant-height and constant-force mode for the manipulation. The simulation of the constant-height mode is straightforward; for a given Z_{tip}, we performed calculations for a large range of X_{tip} values ($\Delta X_{tip} = 0.12$ Å between two steps). The constant-force mode is far more complicated and raises several issues which will be discussed in the last section.
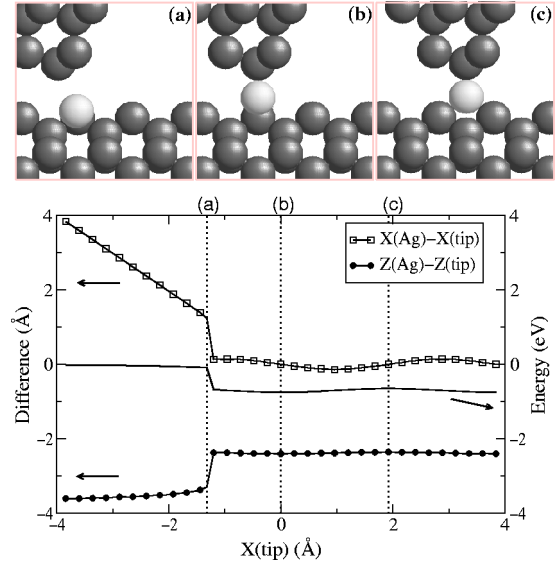

FIG. 3. Example of a surface-to-tip transfer ($Z_{tip} = 3.6$ Å). Upper panel: snapshots for three different tip positions. The dark (light) gray spheres show the Si (Ag) atoms. Lower panel: variation of the X-position difference between the Ag adatom and the tip apex (empty squares), of the height difference between the adatom and the tip apex (filled circles), and of the short-range contributions to the total energy (thick line), Ref. 88. The zero of energy corresponds to the relaxed system with the tip far away from the surface. Only one in two symbols (squares and circles) have been plotted for clarity. The vertical dotted lines mark the tip positions corresponding to the snapshots in the upper panel.

III. CONSTANT-HEIGHT MANIPULATION

In this section, we describe the results obtained in the constant-height mode. In particular, we focused on the conditions required for adatom manipulation. Different kinds of adatom movements have been observed, depending on the tip height, orientation, shape, or chemical nature. However, we considered that a successful manipulation occurred only when the tip translation by a surface lattice parameter leads to an adatom movement in the same direction, and when this process can be successively repeated.

We have been able to obtain four different manipulation mechanisms with our calculations. One is a vertical process where the adatom transfers from the surface to the tip. The three others are the usual lateral manipulation processes, sliding, pulling, and pushing.[25] The upper panel of Fig. 3 shows selected snapshots of the first case. When the tip is still far away from the adatom (on the left of the Fig. 3), one can see that the height difference remains constant and that the X-position difference decreases continuously, i.e., the adatom stays in the cave site, unperturbed by the tip approach. The energy does not vary, meaning that the tip is high enough such that the tip-surface interaction is negligible. At a specific tip position [position (a) in Fig. 3], which depends on the tip height, the configuration becomes energetically unstable, and the adatom "jumps" under the tip apex [position (b) in Fig. 3]. Obviously, we do not have a lateral manipulation since the adatom does not remain on the surface. The mechanism is similar to that depicted for the
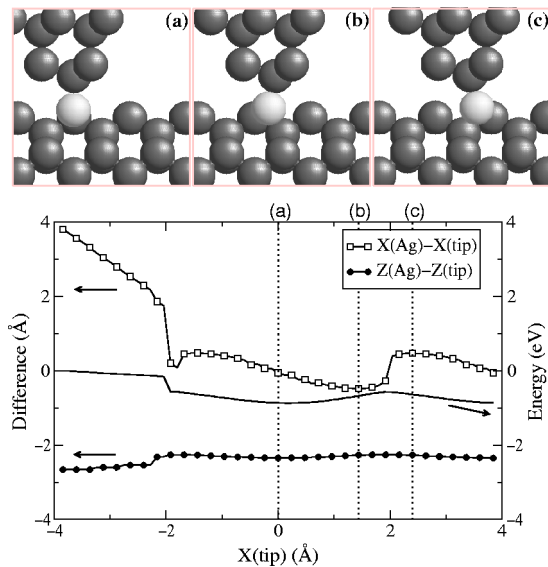
FIG. 4. Example of a sliding process ($Z_{tip}=2.7$ Å). See the caption of Fig. 3 for explanations.

FIG. 5. Example of a pushing process ($Z_{tip}=3.3$ Å). Note that the Si(111) tip is here rotated and that the adatom is initially located in the bond site. See the caption of Fig. 3 for further explanations.

transfer of one atom between two flat electrodes.[32] There are two adsorption minima, one in the cave site and the other under the tip apex, separated by an energy barrier. Because our calculations are done with $T=0$ K, the transition occurs only when the energy barrier vanishes. The transition is clearly visible in the curves, the X-position difference being now almost zero, and the height difference being reduced by 0.9 Å. The energy difference between the two minima, when the tip is far away from the surface, is about 260 meV in favor of adsorption under the tip. It is energetically favored because the adatom is strongly bonded with the dangling orbital on the apex atom of the Si(111) tip. After the transition, the Ag adatom remains attached to the tip apex [positions (b) and (c) in Fig. 3]. Weak undulations of the X-position difference and of the energy prove that the Ag atom still "feels" the surface. The variation of height and energy are perfectly sinusoidal, which Bouju *et al.* have shown to be impossible in the case of a sliding mode, i.e., with the adatom remaining on the surface.[52] The adatom is now clearly bonded only to the tip. Therefore, if the tip is raised, the Ag atom is carried away. However, subsequent deposition may follow if the adatom is brought by the tip in the vicinity of a surface site with a lower adsorption energy, near a step or a kink for instance. Such investigations are beyond the scope of this study.

Lateral manipulation occurred only within three distinct processes.[25] In the sliding mode, the adatom is trapped by the tip apex and follows the tip displacements.[9,25,34,35] It can be obtained if the tip is closer to the surface (Fig. 4). During the tip approach, the adatom jumps again under the apex, and is subsequently trailed by the tip. Unlike the surface-to-tip transfer case, the adatom is still chemisorbed on the surface. Whether or not the tip is more attractive than the surface is no more important in this tip height range, since there is now only one minimum energy position between the tip and the surface. The adatom is pushed back both by the tip and the surface. The only condition for the tip trailing the adatom is
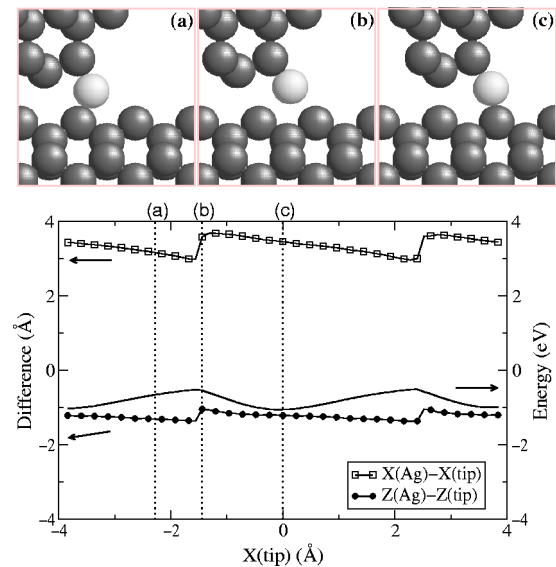
that the potential trap is deep enough to overcome the diffusion barrier on the surface. The X_{Ag}-X_{tip} variation represented in Fig. 4 shows the expected characteristics of a stick-slip behavior,[52] also very well known in the field of friction.[73–79]

Another manipulation process is the pushing mode where the adatom is repelled by the tip displacement. In Fig. 5, an example of pushing is represented for another configuration including a rotated Si(111) tip and the Ag atom initially located in the bond site. Now, the X-position difference ranges from 3 to 4 Å, indicating that the Ag atom is always in front of the moving tip. At the beginning, the distance between the tip and the adatom decreases, since this one prefers to remain in the initial bond site [position (a) in Fig. 5]. It then jumps in the next bond site [position (b) in Fig. 5], and the process is repeated [position (c) in Fig. 5]. The movement of the silver adatom does not appear in the energy curve (Fig. 5). In fact, the energy difference between the two configurations before and after the transition is very small. Instead this is the variation of the tip-surface interaction energy which dominates the curve. The asymmetry of the curve can be explained by the asymmetry of the tip.

In the last process, the manipulated object is pulled by the scanning probe tip (Fig. 6). During the first tip steps, we get a behavior similar to that for the sliding mode. The tip is approaching the silver atom in the cave site, and at some point, this one jumps under the tip [position (a) in Fig. 6]. However, instead to be right under the tip apex, it is now located between the cave site and the tip apex. The tip is too low to allow the adatom to remain permanently under the tip apex. Then, the energy continues to decrease, with a minimum around $X_{tip}=0$ where the tip apex and the adatom are right above the case site. It means that the Ag atom is attracted by both the tip and the surface. Further tip steps lead to an increase in energy whereas the adatom prefers to remain in the vicinity of the cave site. At some point this
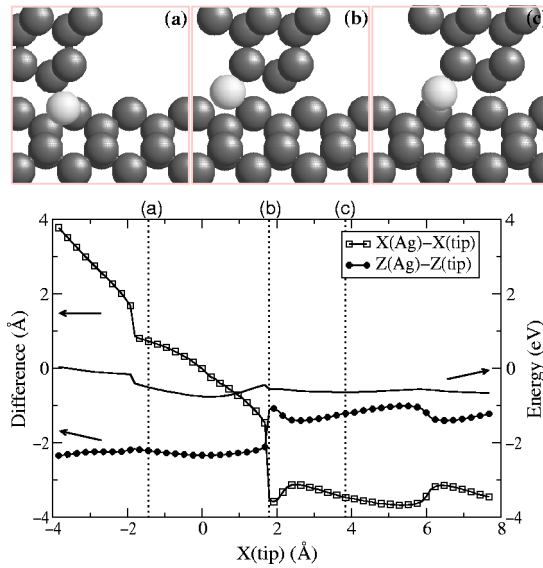
FIG. 6. Example of a pulling process ($Z_{tip}=2.4$ Å). See the caption of Fig. 3 for explanations.

FIG. 7. Results of the scans for all the considered cases $A-G$. For $A-D$ ($E-G$), the Ag adatom is initially located in the cave (bond) site. For each case $A-G$, the column represents the Z_{tip} range corresponding to different adatom behaviors among five. The black color is for a successful pushing mode, the gray one for a surface-to-tip transfer or sliding mode, whereas shaded zones correspond to pulling processes. White and checkerboard areas show unsuccessful manipulations. In the first case (white), the adatom stays in its initial location and in the second case (check board) the adatoms did not remain in line with the tip after the scan. In top ($A-D$) or bottom ($E-G$) of each column, we have represented a side (with the arrow) and a top view of the tip used in each case. White (gray) spheres represent Si (Au) tip atoms.

configuration becomes unstable, and the adatom jumps toward the rear of the tip [position (b) in Fig. 6]. We will show later how this behavior can be correlated with the tip geometry. The adatom is now pulled by the tip during the scan. One can see the nonsinusoidal undulations in the X-position and height differences. The silver adatom feels both the attraction of the tip and of the supporting Si(001) surface. The process includes two distinct steps. In the first step, the adatom goes up and tries to stay close to the stable cave site [position (c) in Fig. 6]. When the tip attraction exceeds the surface attraction, the adatom quickly comes again close to the tip rear. This mode is somewhat peculiar, because the tip has to pass over the adatom in order to trail it. However, the same result could be achieved if the tip is first high above the surface, then lowered in front of the adatom, before the beginning of the scan.

In Fig. 7, we have summarized the results obtained for several cases of constant-height scans, with a tip height ranging from 0.5 Å to 6 Å, with successive increments of 0.1 Å (Si tips) or 0.5 Å (Au tips). With the Ag atom initially in the cave site, we have first considered a Si(111) tip (A), then the same Si tip, but rotated by 120° to have a leading edge (B), an Au(111) tip (C), and finally a truncated Au(111) tip without Au atom at the apex (D). With the Ag atom initially in the bond site, the rotated Si(111) tip was first used (E), then an Au(111) tip (F), and the truncated Au(111) tip (G). The different areas represent Z_{tip} ranges for five different adatom behaviors. Besides the four manipulation processes depicted above, two other cases are emphasized. In the white areas in Fig. 7, the tip passes over the adatom that remains in its initial location, because either the tip is too high or the tip attraction on the adatom is not strong enough to overcome the diffusion barrier. Instead, checkerboard areas gather different unsuccessful behaviors, where the adatom typically avoids the tip by jumping in nearest lateral adsorption sites. Our calculations have been done at $T=0$ K, and one can expect such site hopping's in a larger tip height range in
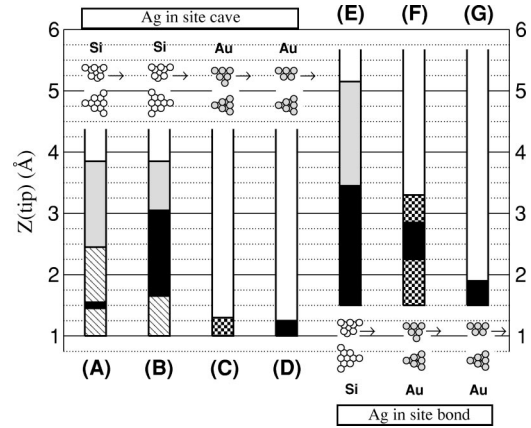
experiments, because of thermal enhancement. This argument emphasizes the need to perform atomic manipulation experiments in a very low temperature environment.

A preliminary study had shown that the manipulation of the Ag adatom on the Si(001) surface was feasible under specific conditions. Indeed, it has been calculated that with a gold tip, pushing occurs within a tip height range between 0.2 and 0.5 Å.[50] This range is may be too small to be certain of the transferability of this result in the experiments, where conditions could be different. However, the overview of our results depicted in Fig. 7 clearly shows that the tip height ranges of successful simulations are typically between 1.5 and 3 Å for the Si tip. This is large enough to ensure that our results are not strongly dependent on the physical approximations we have made. In addition, the controlled manipulation is predicted for different kind of tips and adsorption sites. This is a crucial requirement since despite recent successes in *in situ* structural characterization of the very end of the tip,[80] the geometry of the tip apex is usually not known. Therefore, our results show that with scanning probe techniques one should be able to manipulate one Ag atom on the Si(001) surface.

Several clues about the manipulation on surfaces such as Si(001) can be drawn from the calculations. Here, we found that a sliding process is possible when the tip is made of silicon but not of gold. This result can be explained by the large diffusive energy barrier to overcome on the Si(001) surface. The potential well generated by the Si tip is deep enough to drag the adatom on the surface which cannot be done with an Au tip. In this last case, only the core-core repulsive pushing mode is possible. Another necessary con-
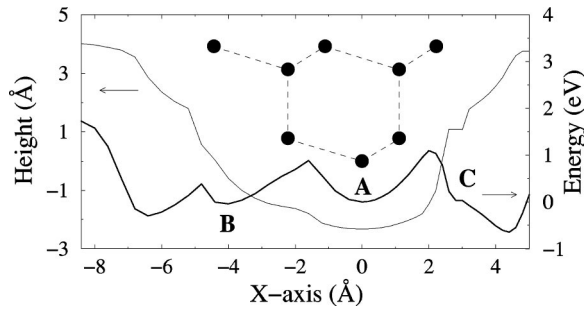
FIG. 8. (X,Z) position and energy of the Ag atom on the isolated Si(111) tip, the atom being at the center of the tip along the Y axis (perpendicular to the scanning direction). The full circles show the tip atom positions (tip apex at the origin) and the letters refer to different minima. The minimum A is the energy reference. Note that if the tip scans to the decreasing X direction and not to the increasing X, it corresponds to the rotated Si(111) tip.

dition to perform manipulation is that the adatom stay in line with in the tip direction. On a surface strongly anisotropic, vicinal with regular steps for instance, this condition can be fulfilled whatever the tip. However, for the Si(001) surface, the adatom must also be guided by the tip. Indeed, the Si tip, with the directional bondings originating from the "s-p" hybridization, prevents in most cases the adatom from escaping aside. On the contrary, the Au tip has a more isotropic adsorption energy surface due to its predominant "s" bonding. It explains why its range of successful pushing is so narrow, the adatom jumping sideways or staying low below the tip.

In Fig. 8, we have represented the position and adsorption energy of the Ag adatom on the isolated Si tip, along the scan direction. We noticed that during the manipulation processes the Ag atom was always located in or very close to a position corresponding to an energy minimum of the energy curve. The minimum labeled A corresponds to the surface-to-tip transfer or sliding mode (Ag under the tip), B to the pulling mode (Ag behind the tip), and C to the pushing mode (Ag in front of the tip). Our results also suggest that the ranges associated with different processes in Fig. 7 depend on the characteristics of these minima. Column (A) of the Fig. 7 shows that sliding and pulling occur for large ranges. Accordingly A and B are deep minima, where the adatom can be accommodated over a large variation of tip height. Conversely, C is a very small minimum, almost an instable point, and it corresponds to the narrow range of tip height of the pushing mode. Further support for this relationship comes by considering column (B) of Fig. 7. Because the Si(111) tip is invariant under the C_3 symmetry operation, Fig. 8 also shows the 120° rotated Si(111) tip if the scan is towards decreasing X. Accordingly, B is now the minimum where the Ag atom is adsorbed during the pushing mode and C during the pulling mode. One clearly sees that because B is a deep minimum, the pushing mode is now possible over a large range. Our suggestion is also supported by the result shown in column (E) of the Fig. 7, where pushing and sliding modes occur over a large similar tip height range. In this last case, the Ag atom is now located in the bond site, which tends to indicate that this criterion may be general whatever the surface, the tip, or the kind of adatom. However, one must be aware that
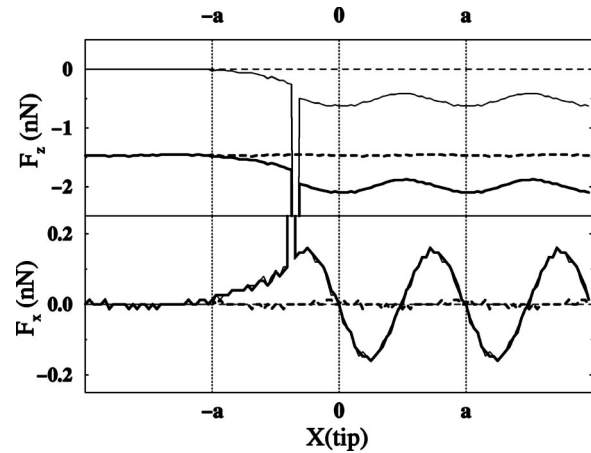

FIG. 9. Variation of the vertical (F_z) and lateral (F_x) forces acting on the tip as a function of the tip position along the dimer row direction for $Z_{tip} = 3.6$ Å. The thick full lines show the forces $F_{z,x}$ with the adatom initially located at $X = 0$, whereas the thick dashed lines represent the forces $F_{z,x}^0$ without the adatom. Also shown with thin lines are the differences $(F-F^0)_{z,x}$. a is the lattice constant-of the Si(001) surface ($a = 3.84$ Å).

these observations remain essentially qualitative and limited to a set of calculations. The success or failure of the manipulation is decided by nontrivial interactions between the surface, adatom, and tip. Our results seem to show that the tip is the essential part of the trio, but more investigations are needed to confirm this phenomenological criterion.

IV. FORCES SIGNATURES

Experiments done by Rieder and co-workers have highlighted that, during constant-current STM manipulation of adatoms, recognizable patterns in response to the tip height signal can be associated with each manipulation process.[35,51] The variations pertaining to each process have been recently reproduced using a numerical simulation of a STM tip and its associated feedback loop device.[52,81] During the manipulation, the object switches between positions alternatively close to or far from the immediate vicinity of the tip apex, what is responsible for the large variations of the extremely sensitive tunneling current. The perturbations caused by the object will not only modify the tunneling current but also the forces acting on the probing tip. We therefore expect to find similar patterns in the force monitored during constant-height scans.

We have calculated the x and z components of the force $\mathbf{F}$ acting on the scanning probe tip, using the computed energy values during a large number of constant-height scans. Once the energy is known on each node of a fine $\{X_{tip}, Z_{tip}\}$ mesh, the forces are derived from the usual formula. For the derivation of F_z, care has been taken to use tip height values close to each other and corresponding to the same manipulation mode. The results for one scan at $Z_{tip} = 3.6$ Å are represented in Fig. 9. When the tip is far from the adatom (left part of the Fig. 9), $\mathbf{F}$ and the tip-surface force $\mathbf{F}^0$ are identical and show negligible variations since the tip is too high to feel the corrugation of the surface. F_z and F_z^0 are not zero because

of the long-range attractive van der Waals contributions. The force on the tip deviates from zero as soon as the distance with the adatom is slightly smaller than a lattice parameter (3.84 Å). F_z decreases whereas F_x increases, the tip being attracted by the adatom. When $X_{tip} = -1.5$ Å, the curve $F_z(X)$ and $F_x(X)$ show discontinuities related to the transfer of the adatom under the tip. These divergences originate from the numerical calculations of the energy derivatives. Once the adatom is located under the tip, we observe oscillations of both F_z and F_x, with the surface lattice periodicity. Actually, the tip is now probing the silicon surface, since the tip is enlarged by the adatom at its apex and is then closer to the surface. The transfer of one adatom under the tip can then be recognized from the increased sensitivity of lateral and vertical forces. An equivalent situation is the sudden increase of contrast obtained with a STM when an adatom initially on the surface transfers under the tip.

The same analysis has been performed for all the configurations considered in the previous part. To get insight into the force variations involved during the manipulation, it is required that **F** has a much larger amplitude than F^0. Figure 10 shows some of the most significant force signatures we have obtained. The upper panel *A* represents the vertical and lateral forces signatures after the adatom has been transferred under the tip. F_z minima occur when the tip carrying the adatom is exactly above the cave sites. Here F_z is lower than F_z^0, which indicates that the force between the tip and the adatom is attractive. F_x is small and is around zero, the adatom being successively attracted by the cave sites in line on the surface. Neither F_z nor F_x shows the typical sawtooth behavior associated with the lateral manipulation. The adatom must stay on the surface in order to introduce an asymmetry in the force variation. The surface-to-tip transfer can then only be recognized by the increased sensitivity of the tip. The central panel *B* shows the forces variations calculated during a sliding process as depicted in Fig. 4. First, one can see that F_z is greater than F_z^0, so the vertical force between the adatom and the tip is repulsive. The most apparent feature of the forces variation is the apparition of asymmetric sawtooth patterns for $F_x(X)$, and also for $F_z(X)$, though more weakly. The analysis of the curves in relation to the adatom positions shows the same kind of stick-slip behavior obtained in STM experiments[35,51] and also well known in the theory of friction.[73–79] Starting with both adatom and tip at the cave site position $[F_x(a)=0$ and $F_z(a)$ close to a minimum], F_x becomes negative and decreases slowly as the tip moves away, the tip being "retained" by the adatom that tries to remain in the cave site. When the tip is ≈ 1.1 Å ahead, the adatom position is instable and it quickly reaches a new position between the tip and the following cave site. F_x suddenly becomes positive whereas the peak in F_z corresponds to the tip and adatom between two cave sites, in a highly repulsive configuration. F_z and F_x then slowly decrease until both the tip and the adatom are again in a cave site. Similar analysis can be done for a pushing process [panel *C* of Fig. 10]. Here, although F_x shows a sharper but similar variation as in the *B* panel, the asymmetry in the oscillation of F_z is now reversed. The slow increase of F_z is
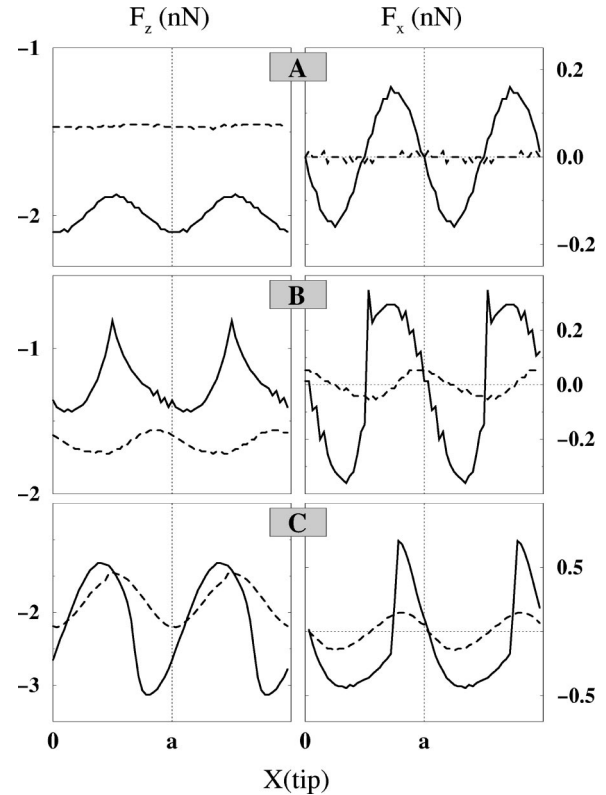

FIG. 10. Variation of the vertical (F_z) and lateral (F_x) forces acting on the tip as a function of the tip position along the dimer row direction for three manipulation processes. The full lines show the forces during the manipulation (**F**) whereas the dashed lines represent the forces without the adatom ($\mathbf{F}^0$). The first case *A* show a surface-to-tip transfer with an attractive vertical force between the adatom and the tip ($Z_{tip} = 3.6$ Å). The case *B* is an example of a sliding process with a repulsive vertical force between the adatom and the tip ($Z_{tip} = 2.8$ Å). Finally *C* show a pushing process [$Z_{tip} = 2.8$ Å, rotated Si(111) tip and adatom in site bond].

associated with the approach of the tip, the contribution of the adatom to F_z being more and more repulsive, and the fast decrease of the force is now caused by the escaping jump of the adatom in the direction of the next bond site.

Constant-current mode STM studies have shown that it is possible to extract the manipulation modes from the tip height variations.[35,51] Figure 10 suggests that the analysis of forces variations could also provide similar and meaningful insights. Tunneling current and interactions are completely different quantities, but it is possible to compare their variations as a function of the tip-surface distance. The tunneling current is a positive scalar quantity, and it approximately changes by one order of magnitude for 1 Å, whatever the nature of the tunneling junction. The distance variation is far more complicated for interaction forces, which can be repulsive or attractive, the latter with either positive or negative gradient. The gradient depends on the nature of the materials,[80,82] and the shape of the tip is also known to have a non-negligible influence.[83–85] In the case of a blunt tungsten tip in interaction with an Au(111) surface, the force gradient has been measured[80] between -4 nN Å^{-1} and $+1$ nN Å^{-1}. We therefore expect that the force signatures

TABLE II. Tip height (constant-current scans) and forces signatures (constant-height scans) during manipulation processes (sliding/pulling and pushing) with a scanning probe tip. We distinguished two cases whether the manipulated object is seen as a depression with STM and the force F_z between the tip and the object varies with a positive gradient (case $\vee$), or the object is seen as a protrusion with STM and the force F_z varies with a negative gradient (case $\wedge$).

		Tip height	F_z	F_x
$\vee$	sliding/pulling	rising sawtooth	rising sawtooth	falling sawtooth
	pushing	falling sawtooth	falling sawtooth	falling sawtooth
$\wedge$	sliding/pulling	falling sawtooth	falling sawtooth	falling sawtooth
	pushing	rising sawtooth	rising sawtooth	falling sawtooth

might show approximate sawtooth shape, unlike the height variations in the STM measurements.

Using our results and deduction, we gathered in Table II the force signatures, just as the tip height signatures reported in STM constant-current experiments, for all the possible cases. We distinguished two cases: whether the force gradient is positive or negative. It is to be noted that two cases must also be considered for the tip height variation in the STM experiments. In fact, it is well known that most of the adsorbates will appear as a protrusion in the constant-current image, effectively increasing the tunneling current, but others will act as a kind of screen for the tunneling and then appear as a depression in the image.[86] The variation shape is then inversed, as was shown in STM experiments.[35] In our calculations, we were unable to obtain the force variations for both sliding/pulling and pushing processes in the positive gradient regime. The adsorption energy minimum being lower on the Si tip, a vertical transfer occurred in the relevant tip height range. The strong attraction of our tip, needed to overcome the large diffusion barrier of the surface, also explains why the calculated force signatures are not as sharp as in Table II. During the manipulation, most of the time the adatom remained in the proximity of the apex, and the lateral jumps to the next site were small. Larger jumps would greatly enhance the sharpness of the signature patterns.

The force signatures compiled in Table II could first help to determine if manipulation occurred. Indeed, a sudden increase of the asymmetry of F_x variation means that the tip push or drag an object on the surface. Also, the increase of the amplitude of the F_z variation may be associated with a transfer of the object under the tip. Manipulation processes could also be recognized from the analysis of the F_z sawtooth variations. Once the relation between the force and the tip-surface distance is determined, i.e., we know if the gradient is positive or negative, it should be relatively easy to deduce if sliding/pulling or pushing had occurred during the scan.

V. CONSTANT-FORCE MANIPULATION

Theoretical studies of the manipulation of one atom by a scanning probe tip usually focused on the constant-height mode. Its simulation is easier than for modes based on the control of one interaction quantity, such as constant current in STM or constant force in AFM. Indeed, in constant-height mode, there is no need to take into account the effect of a feedback loop on the scanning tip. To our knowledge, the first attempt to simulate other modes has been achieved by Bouju *et al.*[52] With their *virtual* scanning tunneling microscope, they were able to reproduce the sawtooth variation of the STM tip height during the constant-current manipulation of a Xe atom on a Cu(110) surface. However, as far as we know, other modes, such as AFM constant force, have not been investigated yet in the purpose of manipulation. From the experimental point of view, no reports of manipulation in constant-force mode have been made. The occurrence of the so-called snap-to-contact due to mechanical instabilities when the force gradient $\partial F_z/\partial z$ exceeds the cantilever stiffness for small tip surface separation may be one of the inherent difficulties.[87] Therefore, numerical simulations are an invaluable tool to investigate the manipulation mechanisms in this mode.

The straightforward way to simulate constant-force scans consists in implementing an extra algorithm in the computational code, which mimics the feedback loop. First, we have tried this approach. We made the assumption that the characteristic time of the adatom relaxation is much smaller than the feedback loop response, i.e., the time required to adjust the height of the tip. Practically, the adatom position is then fully relaxed for each tip height, which corresponds to the adatom following adiabatically the tip vertical movement. *A low tip speed adjustment is needed in order to avoid large oscillations of the tip, which may lead to tip crashing or lateral adatom jumps.* Although less elaborate, this scheme is equivalent to the technique used for the virtual scanning tunneling microscope.[52] However, this automatic technique shows several drawbacks for constant-force mode. In the useful range, the variation of the force between the tip and the surface as a function of the tip height is not monotonic, unlike the variation of the tunneling current with the distance. This problem can be tackled by a careful optimization of the speed of the tip height adjustment. Hence, we were able to obtain constant-force scans of the bare surface using
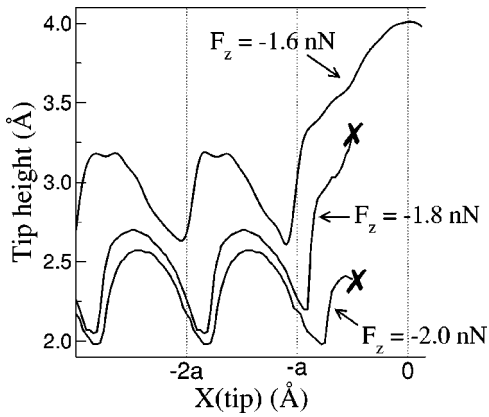
FIG. 11. Constant-force scans for $F_z = -1.6$ nN, -1.8 nN, and -2 nN (positive force gradient) with a Si(111) tip and the Ag atom in the cave site. The crosses mark the tip position at which the adatom jumps under the tip. Note that the adatom is initially located at $X_{tip} = 0$.
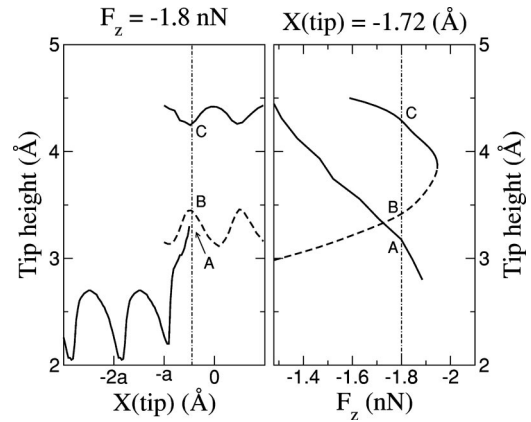

FIG. 12. Left panel: Tip height variations as a function of the tip position for a constant-force $F_z = -1.8$ nN scan, before and after the transition [marked by the dashed curve at $X(tip) = -1.72$ Å]. Right panel: Tip height variations as a function of the vertical force F_z for the tip position $X(tip) = -1.72$ Å. For the curves labeled A, the adatom remains in its initial adsorption site [$X(tip) = 0$ Å], whereas it is located under the tip for B (negative force gradient, $\partial F_z / \partial z < 0$) and C (positive force gradient, $\partial F_z / \partial z > 0$) curves.

this technique. However, additional difficulties appear when the scanning tip interacts with the supported adatom. For example, a jump of the adatom directly under the tip may drastically change the interaction between the tip and surface. In the tip height range useful for the manipulation, an attractive vertical force will be repulsive after the jump, which will result in instabilities in the feedback loop.

Therefore, in this work, we favored another approach, with which these instabilities are clearly identified. Practically, we used the vertical force between the tip and surface calculated for each X_{tip}, Z_{tip} on a fine grid. The sequence of the tip heights Z_{tip} during a scan is then extracted for successive X_{tip} from this set by assuming a constant- force. When an instability occurs, for example, because of an adatom jump under the tip apex, we then consider a new set of positions and forces associated with the new tip configuration, i.e., with the adatom located under the tip. The advantage of this method is the possibility to get all the solutions for a given force. In particular, we can analyze precisely the behavior of the system near a feedback instability.

Figure 11 shows tip height variations calculated for several force values in the case of a Si(111) tip and the Ag adatom in the cave site. Far from the neighborhood of the adatom, we have obtained height variations with the periodicity of the Si(001) substrate, with asymmetric shapes reflecting the nonsymmetric configuration of the tip. The minimum heights occurred close to the cave sites locations. For $F_z = -1.6$ nN, the tip still did not "feel" the adatom until X_{tip} is approximately lower than $-a$. After this position, the tip rose because of the increasing interaction with the adatom. The tip then passed over the adatom with $Z_{tip} = 4$ Å, high enough to prevent a surface-to-tip transfer. The higher bump at $X_{tip} = 0$ is the image of the Ag atom in the constant-force mode. However, for $F_z = -1.8$ nN or $F_z = -2.0$ nN, the tip is closer to the surface during the scan, and the adatom jumped under the tip apex when $X_{tip} \simeq -a/2$. In the normal conditions, the slow motion of the tip holder causes gradual changes. But here, the adatom jump completely

changes the value of F_z, and mechanical instabilities are expected to follow.

Now we focus on the effect of the surface-to-tip jump of the adatom during the scan at $F_z = -1.8$ nN. Owing to the much longer response times of the cantilever and the feedback, the final outcome can be determined from the static $F_z(z)$ at the location of the adatom jump. We reported in Fig. 12 the possible tip trajectories. The left graph shows the tip height variation before the jump, reported from Fig. 11. At the jump [$X(tip) = -1.72$ Å], the adatom is transferred under the tip. The right graph of Fig. 12 represents how the tip height varies as a function of the force at the transition point. The curve A corresponds to the configuration with the adatom on the cave site, whereas for B and C, the adatom is now located at the tip apex. The intersection of the curves with the dashed line gives the tip height for each configuration. After the jump, there are two solutions, one for the branch B (negative force gradient) and the other for the branch C (positive force gradient). We have to examine the two possible transitions $A \rightarrow B$ and $A \rightarrow C$. The corresponding continuations of the scan are shown in the left graph of Fig. 11. First, we considered the transition $A \rightarrow B$. At B, the force gradient is negative, unlike the configuration A. Because the feedbacks are usually assumed by design to keep the sign of the force gradient, a slow instability of the tip holder is expected, followed by a crash on the surface. The other possible transition, $A \rightarrow C$, does not suffer the gradient restriction. At A, before the adatom jump, the tip-cantilever system is in equilibrium, the attraction by the surface being balanced by the return force of the cantilever. Right after the adatom transfer, the tip-surface force becomes suddenly repulsive and adds up with the return force to raise the tip. The tip will oscillate around the new equilibrium position with a maximum amplitude equal to the difference between the initial and final positions. Here, the height difference between A

and C is about 1 Å. If we assume that the adatom remains in its location at the tip apex during the oscillations and that the feedback speed is much greater than the scan speed, these oscillations will be progressively dampened and the slow compensation by the feedback loop will bring the tip to the new equilibrium position. The scanning will then continue with the height variations shown on the branch C in the left graph of the Fig. 12.

For the system we have considered, in the range of attractive force with a positive gradient, we observed that either the tip images the adatom or a surface-to-tip transfer happened during the scan over the adatom. Other possibilities, encompassing attractive forces with negative gradient, repulsive forces, or different tip shapes and orientations have not been fully investigated; an exhaustive study being out of the scope of the present paper and could be the matter of a future publication. However, we emphasize that our analysis remains valid for the general case since we have always observed a jump of the adatom during the approach of the tip.

VI. CONCLUSION

We have investigated the manipulation by a scanning probe tip of one silver atom deposited on a Si(001) surface using a molecular mechanics approach. The system was described by a cluster model, and we have used the combination of a quantum chemistry model for the short-range interactions and an analytical Hamaker model for the long-range van der Waals contributions. We have identified four different possible manipulation processes, i.e., the surface-to-tip transfer, the sliding, pulling, and pushing modes, when using a Si(111) tip, whereas only pushing is achieved in the case of an Au tip. The structure of the tip apex has been shown to be the predominant factor for determining the ordering and tip height ranges associated with each manipulation process. The second part of the paper was devoted to an original study of the forces variations during the manipulation. We have determined that each process is associated with characteristic variations, very similar to the height signatures observed in constant-current STM experiments. It is suggested that the kind of process involved in the manipulation could be inferred from the monitoring of the forces. Finally, we have presented the numerical simulations of the AFM constant-force mode. From a preliminary analysis, the different possible behaviors of the tip during a surface-to-tip transfer are discussed, taking into account the feedback and cantilever responses.

*Author to whom correspondence should be sent. FAX: 33 549 496 692. Email address: Laurent.Pizzagalli@univ-poitiers.fr

[1] G. Binnig, H. Rohrer, C. Gerber, and E. Weibel, Phys. Rev. Lett. **49**, 57 (1982).

[2] G. Binnig, C.F. Quate, and C. Gerber, Phys. Rev. Lett. **56**, 930 (1986).

[3] H.K. Wickramasinghe, in *Scanning Tunneling Microscopy*, edited by A. Stroscio and W.J. Kaiser, *Methods of Experimental Physics*, Vol. 27 (Academic Press, San Diego, 1993), Chap. 3, p. 77.

[4] G. Binnig and H. Rohrer, Rev. Mod. Phys. **71**, S324 (1999).

[5] Y.Z. Li, L. Vazquez, R. Piner, R.P. Andres, and R. Reifenberger, Appl. Phys. Lett. **54**, 1424 (1989).

[6] H. Fuchs, R. Laschinski, and T. Schimmel, Europhys. Lett. **13**, 307 (1990).

[7] T. Schimmel, H. Fuchs, and M. Lux-Steiner, Phys. Status Solidi A **131**, 47 (1992).

[8] H.J. Mamin, P.H. Guethner, and D. Rugar, Phys. Rev. Lett. **65**, 2418 (1990).

[9] D.M. Eigler and E.K. Schweizer, Nature (London) **344**, 524 (1990).

[10] J.A. Stroscio and D.M. Eigler, Science **254**, 1319 (1991).

[11] I.-W. Lyo and P. Avouris, Science **253**, 173 (1991).

[12] P. Avouris, I.-W. Lyo, and Y. Hasegawa, in *Atomic and Nanometer-Scale Modification of Materials: Fundamentals and Applications*, Vol. 239 of *NATO Advanced Studies Institute Series E: Applied Sciences*, edited by P. Avouris (Kluwer Academic, Dordrecht, 1993), p. 11.

[13] A. Kobayashi, F. Grey, H. Uchida, D.-H. Huang, and M. Aono, in *Atomic and Nanometer-Scale Modification of Materials: Fundamentals and Applications* (Ref. 12), p. 37.

[14] F. Grey, D. Huang, and M. Aono, Philos. Mag. B **70**, 711 (1994).

[15] S. Hosaka, S. Hosoki, T. Hasegawa, H. Koyanagi, T. Shintani, and M. Miyamoto, J. Vac. Sci. Technol. B **13**, 2813 (1995).

[16] T.-C. Shen, C. Wang, G.C. Abeln, J.R. Tucker, J.W. Lyding, P. Avouris, and R.E. Walkup, Science **268**, 1590 (1995).

[17] P. Avouris, Acc. Chem. Res. **28**, 95 (1995).

[18] D. Huang, F. Grey, and M. Aono, Jpn. J. Appl. Phys., Part 1 **34**, 3373 (1995).

[19] C.T. Salling, J. Vac. Sci. Technol. B **14**, 1322 (1996).

[20] T.-C. Shen and P. Avouris, Surf. Sci. **390**, 35 (1997).

[21] D.H. Huang and M. Aono, J. Surf. Anal. **3**, 264 (1998).

[22] G. Dujardin, A. Mayne, O. Robert, F. Rose, C. Joachim, and H. Tang, Phys. Rev. Lett. **80**, 3085 (1998).

[23] D.M. Eigler, C.P. Lutz, and W.E. Rudge, Nature (London) **352**, 600 (1991).

[24] D. Eigler, in *Atomic and Nanometer-Scale Modification of Materials: Fundamentals and Applications* (Ref. 12), p. 1.

[25] G. Meyer and K.-H. Rieder, Surf. Sci. **377-379**, 1087 (1997).

[26] G. Meyer, L. Bartels, and K.-H. Rieder, Comput. Mater. Sci. **20**, 443 (2001).

[27] C. Joachim, P. Sautet, and P. Lagier, Europhys. Lett. **20**, 697 (1992).

[28] C. Girard, X. Bouju, and C. Joachim, Chem. Phys. **168**, 203 (1992).

[29] C. Joachim, X. Bouju, and C. Girard, in *Nanosources and Manipulations of Atoms Under High Fields and Temperatures: Applications*, Vol. 235 of *NATO Advanced Studies Institute Series E: Applied Sciences*, edited by V.T. Binh, N. Garcia, and K. Dransfeld (Kluwer Academic, Dordrecht, 1993), p. 1.

[30] N. Lang, in *Atomic and Nanometer-Scale Modification of Materials: Fundamentals and Applications* (Ref. 12), p. 87.

[31] T.T. Tsong and C.-S. Chang, Jpn. J. Appl. Phys., Part 1 **34**, 3309 (1995).

[32] A. Buldum and S. Ciraci, Phys. Rev. B **54**, 2175 (1996).

[33] K. Stokbro, C. Thirstrup, M. Sakurai, U. Quaade, B.Y.-K. Hu, F. Perez-Murano, and F. Grey, Phys. Rev. Lett. **80**, 2618 (1998).

[34] P. Zeppenfeld, C.P. Lutz, and D.M. Eigler, Ultramicroscopy **42-44**, 128 (1992).

[35] L. Bartels, G. Meyer, and K.-H. Rieder, Phys. Rev. Lett. **79**, 697 (1997).

[36] P.H. Beton, A.W. Dunn, and P. Moriarty, Appl. Phys. Lett. **67**, 1075 (1995).

[37] T. Junno, K. Deppert, L. Montelius, and L. Samuelson, Appl. Phys. Lett. **66**, 3627 (1995).

[38] T.A. Jung, R.R. Schlittler, J.K. Gimzewski, H. Tang, and C. Joachim, Science **271**, 181 (1996).

[39] M.T. Cuberes, R.R. Schlittler, and J.K. Gimzewski, Appl. Phys. Lett. **A69**, 3016 (1996).

[40] M.T. Cuberes, R.R. Schlitter, and J.K. Gimzewski, Appl. Phys. A: Mater. Sci. Process. **66**, S669 (1998).

[41] C. Baur, A. Bugacov, B.E. Koel, A. Madhukar, N. Montoya, T.R. Ramachandran, A.A.G. Requicha, R. Resch, and P. Will, Nanotechnology **9**, 360 (1998).

[42] S. Jay Chey, L. Huang, and J.H. Weaver, Phys. Rev. B **59**, 16 033 (1999).

[43] L.J. Whitman, J.A. Stroscio, R.A. Dragoset, and R.J. Celotta, Science **251**, 1206 (1991).

[44] X. Bouju, M. Devel, and C. Girard, Appl. Phys. A: Mater. Sci. Process. **A66**, S749 (1998).

[45] G. Meyer, L. Bartels, S. Zöphel, and K.H. Rieder, Appl. Phys. A: Mater. Sci. Process. **A68**, 125 (1999).

[46] X. Bouju, C. Joachim, C. Girard, and P. Sautet, Phys. Rev. B **47**, 7454 (1993).

[47] X. Bouju, C. Girard, H. Tang, C. Joachim, and L. Pizzagalli, Phys. Rev. B **55**, 16 498 (1997).

[48] U. Kürpick and T.S. Rahman, Phys. Rev. Lett. **83**, 2765 (1999).

[49] X. Bouju, C. Joachim, and C. Girard, Phys. Rev. B **50**, 7893 (1994).

[50] L. Pizzagalli, J. Okon, and C. Joachim, Surf. Sci. Lett. **384**, L852 (1997).

[51] L. Bartels, G. Meyer, and K.-H. Rieder, Chem. Phys. Lett. **273**, 371 (1997).

[52] X. Bouju, C. Joachim, and C. Girard, Phys. Rev. B **59**, R7845 (1999).

[53] D. Badt, H. Wengelnik, and H. Neddermeyer, J. Vac. Sci. Technol. B **12**, 2015 (1994).

[54] H. Tochihara, T. Amakusa, and M. Iwatsuki, Phys. Rev. B **50**, 12 262 (1994).

[55] A.W. Munz, C. Ziegler, and W. Göpel, Phys. Rev. Lett. **74**, 2244 (1995).

[56] D.J. Chadi, Phys. Rev. Lett. **43**, 43 (1979).

[57] N. Roberts and R.J. Needs, Surf. Sci. **236**, 112 (1990).

[58] A. Ramstad, G. Brocks, and P.J. Kelly, Phys. Rev. B **51**, 14 504 (1995).

[59] A. Samsavar, E.S. Hirschorn, F.M. Leibsle, and T.-C. Chiang, Phys. Rev. Lett. **63**, 2830 (1989).

[60] T. Hashizume, R.J. Hamers, J.E. Demuth, K. Markert, and T. Sakurai, J. Vac. Sci. Technol. A **8**, 249 (1990).

[61] X.F. Lin, K.J. Wan, and J. Nogami, Phys. Rev. B **47**, 13 491 (1993).

[62] D. Winau, H. Itoh, A.K. Schmid, and T. Ichinokawa, J. Vac. Sci. Technol. A **12**, 2082 (1994).

[63] K. Kimura, K. Ohshima, and M. Mannami, Phys. Rev. B **52**, 5737 (1995).

[64] J.C. Okon and C. Joachim, Surf. Sci. Lett. **376**, L409 (1997).

[65] T. Yakabe, Z.-C. Dong, and H. Nejoh, J. Surf. Anal. **3**, 346 (1998).

[66] K. Nath and A.B. Anderson, Phys. Rev. B **41**, 5652 (1990).

[67] S. Ciraci and H. Wagner, Phys. Rev. B **27**, 5180 (1983).

[68] H. Tang, C. Joachim, and J. Devillers, Europhys. Lett. **30**, 289 (1995).

[69] C. Argento and R.H. French, J. Appl. Phys. **80**, 6081 (1996).

[70] The cone angle is $\gamma = 0.5137$ rad. With this value, the cone shape is equivalent to a pyramidal shape with an aspect ratio 1:1 (see Ref. 69).

[71] T.J. Senden and C.J. Drummond, Colloids Surf., A **94**, 29 (1995).

[72] H. Tang, M.T. Cuberes, C. Joachim, and J.K. Gimzewski, Surf. Sci. **386**, 115 (1997).

[73] E. Meyer and H. Heinzelmann, in *Scanning Tunneling Microscopy II*, edited by R. Wiesendanger and H.-J. Güntherodt, Vol. 28 of Surface Sciences (Springer-Verlag, Berlin, 1992), Chap. 4, p. 99.

[74] O. Marti, J. Colchero, and J. Mlynek, in *Nanosources and Manipulations of Atoms Under High Fields and Temperatures: Applications* (Ref. 29), p. 253.

[75] T. Gyalog, M. Bammerlin, R. Lüthi, E. Meyer, and H. Thomas, Europhys. Lett. **31**, 269 (1995).

[76] D. Tománek, in *Scanning Tunneling Microscopy III*, edited by H.-J. Güntherodt and R. Wiesendanger, Vol. 29 of Surface Sciences (Springer-Verlag, Berlin, 1996), Chap. 11.

[77] R.W. Carpick and M. Salmeron, Chem. Rev. (Washington, D.C.) **97**, 1163 (1997).

[78] H. Hölscher, U.D. Schwarz, and R. Wiesendanger, Surf. Sci. **375**, 395 (1997).

[79] J. Shimizu, H. Eda, M. Yoritsune, and E. Ohmura, Nanotechnology **9**, 118 (1998).

[80] G. Cross, A. Schirmeisen, A. Stalder, P. Grütter, M. Tschudy, and U. Dürig, Phys. Rev. Lett. **80**, 4685 (1998).

[81] X. Bouju, C. Joachim, C. Girard, and H. Tang, Phys. Rev. B **63**, 085415 (2001).

[82] J.H. Rose, J. Ferrante, and J.R. Smith, Phys. Rev. Lett. **47**, 675 (1981).

[83] S. Ciraci, A. Baratoff, and I.P. Batra, Phys. Rev. B **41**, 2763 (1990).

[84] H. Ness, D. Stoeffler, and F. Gautier, Surf. Sci. Lett. **294**, L969 (1993).

[85] R. Pérez, M.C. Payne, I. Štich, and K. Terakura, Phys. Rev. Lett. **78**, 678 (1997).

[86] This point is dicussed in detail in G.A.D. Briggs and A.J. Fisher, Surf. Sci. Rep. **33**, 1 (1999).

[87] The use of force-controlled feedback loops should overcome this problem. See, for example, S.P. Jarvis, H. Yamada, S.-I. Yamamoto, H. Tokumoto, and J.B. Pethica, Nature (London) **384**, 247 (1996).

[88] During the manipulation, the adatom remained almost in line with the tip, and therefore we have not represented the variation of the adatom position in the direction perpendicular to the tip movement.